Biofidelity Corridors for Whole-Body Pedestrian Impact with a Generic Buck

Jason L. Forman, Hamed Joodaki, Ali Forghani, Patrick Riley, Varun Bollapragada, David Lessley, Brian Overby, Sara Heltzel, Jeff Crandall

Abstract Efforts to develop a dummy capable of assessing injury risk in a pedestrian collision require biofidelity assessment targets in full-scale pedestrian-impact scenarios. The goal of this study was to develop trajectory analysis methods and kinematic biofidelity corridors for 50th percentile male adults subjected to 40 km/h pedestrian impacts using a recently-developed generic sedan buck. Tests were performed with three male post-mortem human surrogates initially positioned to be struck laterally in a mid-gait stance. The kinematics of the post-mortem human surrogates were recorded via high-speed video imagers and a 3D optoelectronic motion capture system. Trajectories of the head center of gravity, T1, T8, and the pelvis were digitized via a 2D video (up to the time of head impact). The 2D trajectory data were verified against comparable measures from the 3D motion tracking system. These data were then scaled to a 50th percentile adult male and corridors for the scaled trajectories were developed. Combined with the generic vehicle buck and validated trajectory capture and analysis methods, these results provide a means to evaluate the whole body kinematic biofidelity of 50th percentile male pedestrian dummies and computational models in perpetuity.

Keywords biofidelity, cadaver, dummy, experiments, pedestrian

I. INTRODUCTION

Pedestrian collisions account for 270,000 annual traffic fatalities worldwide [1]. Reduction will require a combination of efforts, including roadway environment design, pedestrian collision avoidance, and passive protection via vehicle crashworthiness for pedestrian protection. Current standardized test programs for pedestrian passive safety evaluation focus on component-level evaluation via impactor tests [2]. While these can provide valuable information, they lack the ability to assess the aspects of pedestrian-vehicle interaction that are affected by interactions between the various body regions. For example, [3] found that common adult headform pedestrian impactor tests tended to underestimate head acceleration and Head Injury Criterion (HIC) compared to full-scale (whole-body) pedestrian impact tests performed with post-mortem human surrogates (PMHS, cadavers). The authors hypothesized that this difference resulted in fundamentally different kinetic behaviors between the impactor and the full scale test due to interaction of the head with the neck and torso (in whole-body impacts the neck and torso apply an additional accelerating force to the head that is not captured by the impactor tests). Similar differences may be seen in the lower extremity impactor tests and whole-body tests, also resulting from interactions with the other body regions resulting in inertial boundary conditions that cannot be replicated using an impactor alone. These factors are especially problematic in the development and evaluation of advanced passive pedestrian systems such as pop-up hoods and pedestrian airbags. Because these technologies interact with multiple body regions and affect overall subject kinematics, their effect on injury risk cannot be fully assessed using impactor tests alone [4].

Thorough evaluation of passive pedestrian safety requires the availability of validated pedestrian dummies and computer models that may be used to assess injury risk under full-scale, whole-body impact. To address this need, in 2010 the Society of Automotive Engineers published a set of technical standards to provide guidance for pedestrian dummy anthropometry design and biofidelity assessment. SAE J2782 [5] "Performance

Jason Forman is a Principal Scientist in Mechanical and Aerospace Engineering (phone: +1-434-296-7288; fax: +1-434-296-3453; email: jlf3m@virginia.edu). Hamed Joodaki and Varun Bollapragada are Ph.D. students in Mechanical Engineering. Ali Forghani is a Research Specialist. Patrick Riley is a Research Scientist. David Lessley is a Research Associate. Brian Overby is a Research Engineer. Sara Heltzel is Biological Material Specialist. Jeff Crandall is a Nancy and Neal Wade Professor of Engineering and Applied Sciences. All authors are affiliated with the University of Virginia Center for Applied Biomechanics.

Specifications for a Midsize Male Pedestrian Research Dummy" provides specifications for anthropometry and component-level validation, including head and neck biofidelity, shoulder response, torso response, knee bending response, tibia bending response, and inertial characteristics for the various body regions. However, to ensure that such a model is capable of accurately reproducing the complex interaction with a vehicle present in pedestrian collisions, it must also exhibit biofidelity on a whole-body level. To address this, SAE J2868 [6] "Pedestrian Dummy Full Scale Test Results and Resource Materials" describes biofideltiy corridors for the trajectories of the head, first thoracic vertebra (T1, upper spine), eighth thoracic vertebra (T8, midspine), and pelvis for full-scale (whole-body) pedestrian impact tests. Those trajectory response corridors were developed from full-scale sled tests performed with mid-sized male PMHS with a vehicle impact speed of 40 km/h. In those tests the striking article consisted of the front end of a 2004 four-door Honda Civic mounted to an impact sled.

While those tests have provided valuable information, the integration of a specific production vehicle as equipment used in a dummy evaluation standard is problematic. Doing so would rely on future dummy developers having access not only to that vehicle, but also to all the replacement parts necessary to repair the damage that occurs during each test. To address this, members of the SAE Pedestrian Dummy Task Group (PDTG) have developed a simplified pedestrian vehicle buck designed specifically for dummy and model biofidelity assessment [7-9]. This buck is constructed with relatively simple geometries and materials which may be specified in a manner such that it will be reproducible in perpetuity (Figure 1). The development of the buck is described in detail by Pipkorn et al. [7-8] and Takahashi et al. [9]. In brief, the buck is composed of a set of deformable interaction components (upper bumper, lower bumper, grill, hood leading edge, hood, windshield) mounted on a rigid frame. The combined contour of the interaction components is designed based on the average of 16 small European family cars [7-8]. Each interaction component is constructed of simple engineering materials (e.g., polyethylene, sheet steel, etc.) with the bumper, grill, and hood stiffnesses designed to be representative of a good rated vehicle in EuroNCAP pedestrian impactor testing.

The goal of this study was to generate trajectory biofidelity corridors for whole-body pedestrian impact tests performed with the generic sedan buck. Targeting the development of a dummy/model biofidelity standard, this study also sought to develop trajectory measurement and analysis methods that could be reproduced by other laboratories. These trajectory measurement and analysis methods were validated through comparison with results derived from high-speed 3D motion capture.

II. METHODS

Test Setup

The pedestrian test method used here was described in detail by Kerrigan et al. [10] and Kam et al. [11]. In short, tests were performed on a deceleration-type sled system wherein the striking vehicle buck was mounted to a sled carriage and propelled into a standing test subject. The vehicle sled and subject were allowed to interact for approximately 250 ms, after which the vehicle sled was decelerated and the test subject was caught by an energy absorbing net. All tests were performed with a target impact velocity of 40 km/h.

All tests were performed using a VIA Systems model 713 deceleration sled. Each of the interaction components of the buck were replaced following each test. The materials and nominal thicknesses (i.e., thicknesses under which these materials are marketed by their various suppliers) of the bumpers, grill, hood leading edge, and hood are listed in Table I. For this study the goal was to observe the kinematic response from the time of leg contact to the time of head contact. It was not necessarily the intention to capture the interaction of the head with the windshield post-contact, so a simplified non-frangible windshield material was used. The windshield consisted of a 1000x1390 mm piece of Lexan model 9030, with a nominal (marketed) thickness of 8 mm. The buck was rigidly mounted to the VIA systems sled carriage, and was ballasted up to a total test weight of 1175 kg (buck+carriage+other mounted components; Figure 1).

Fig. 1. Photo of the buck prepared and mounted to the sled.

TABLE I
BUCK COMPONENT NOMINAL MATERIAL THICKNESS

Component	Material	Nominal Material Thickness (mm)
Hood	Steel*	0.75
Hood edge	Steel	1.0
Grille	Polyethylene	2.0
Upper Bumper (inner and outer)	Polyethylene	2.0
Lower Bumper (inner and outer)	Polyethylene	1.5

* The hood component also included a formed structural backing around its perimeter.

Test Subjects and Preparation

Test subjects consisted of three male PMHSs. The subjects were acquired and prepared in accordance with the UVA Center for Applied Biomechanics Oversight Committee. The subjects were preserved by freezing and confirmed free of infectious diseases including HIV and Hepatitis B and C. Full-body computed tomography (CT) scans were taken of each subject prior to testing to confirm the absence of bony trauma. Dual-energy X-ray absorptiometry (DXA) was also used to assess bone quality. Subjects were screened for anthropometry targeting a 50th percentile adult male. Summary subject information is included in Table II, and detailed anthropometry measurements are included in Appendix A.

TABLE II
TEST SUBJECT INFORMATION (ALL SUBJECTS MALE)

Test #	Subject #	Age	Stature (cm)	Body Mass (kg)	Cause of Death
V2370	M724	73	179.5	72.6	Heart Failure
V2371	M727	54	187.0	81.6	Colon Cancer
V2374*	M756	67	178.0	78.0	COPD

* This subject had its distal upper extremities amputated bilaterally at the mid-forearm.

The PMHSS were prepared by installing instrumentation and photo target mounts on the head, T1, T8, pelvis, distal femurs, proximal tibias, and distal tibias. The spine and head mounts were secured to the skeleton via wood screws placed into the bone. The femur and tibia mounts were installed via steel hose clamps secured around the bones. Each of these mounts included a small platform onto which accelerometer packages were installed, as well as provisions for the attachment of aluminum standoffs onto which external Vicon and phototarget marker arrays were later attached. The details of the mounts and marker plate systems are similar to that described by Shaw et al. [12] and Lessley et al. [13]. On test days, after the instrument packages and marker plate standoffs were installed the incision sites were closed and the subjects were wrapped entirely with a single layer of Coban^{TM} (3M^{TM}) self-adhesive wrap (as described in Forman et al. [14]). Coban^{TM} is a thin, highly-extensible, elastic wrap that is commonly used in clinical applications to affix dressings and secure instrumentation leads and other devices. While Coban^{TM} is sometimes used in multiple layers to form an athletic joint-support bandage, it does not substantially affect joint flexibility when used in moderation (e.g., one to two layers). This technique has been used previously in cadaver sled test studies [12-14]. After wrapping in Coban, the subjects were clothed with a 65% cotton, 35% polypropylene blend thermal undergarment and with general-purpose athletic shoes. The total mass of all equipment added to the subjects was approximately 7.4 kg (including instrumentation, data acquisition, cabling, and Vicon hardware; excluding clothing and shoes).

Initial Positioning

The subjects were initially positioned in a nominal mid-gait stance with the right foot back and the left foot forward, and were oriented relative to the buck such that they were struck laterally on the subject's right side (Figure 2). The arms were positioned with the hands crossed in front of the abdomen and bound at the wrist with cable ties (for test V2374, the upper extremities were bound together at the point of amputation). For each subject the initial position was adjusted targeting the positioning guidelines described in SAE J2782, particularly targeting the left and right femur angles and tibia angles, torso angle, and head angle (Appendix B). The position was adjusted when necessary for stability and to balance between different measurement targets.

Each subject's vertical position was adjusted to align the struck-side knee at a prescribed target height relative to the buck ground reference plane. In a simulation sensitivity study Yanaoka et al. [15] found that aligning different size subjects based on knee height and then applying length scaling produced more consistent trajectory results compared to length scaling alone (i.e. with no vertical position adjustment). In these tests, this vertical position adjustment was accomplished by raising or lowering the subject's foot platform via stiff foam spacers. The target vertical knee position was 505 mm above the buck ground reference plane, as suggested by SAE J2782. The required adjustments are shown in Table III. The resulting positions are illustrated in Figure 3.

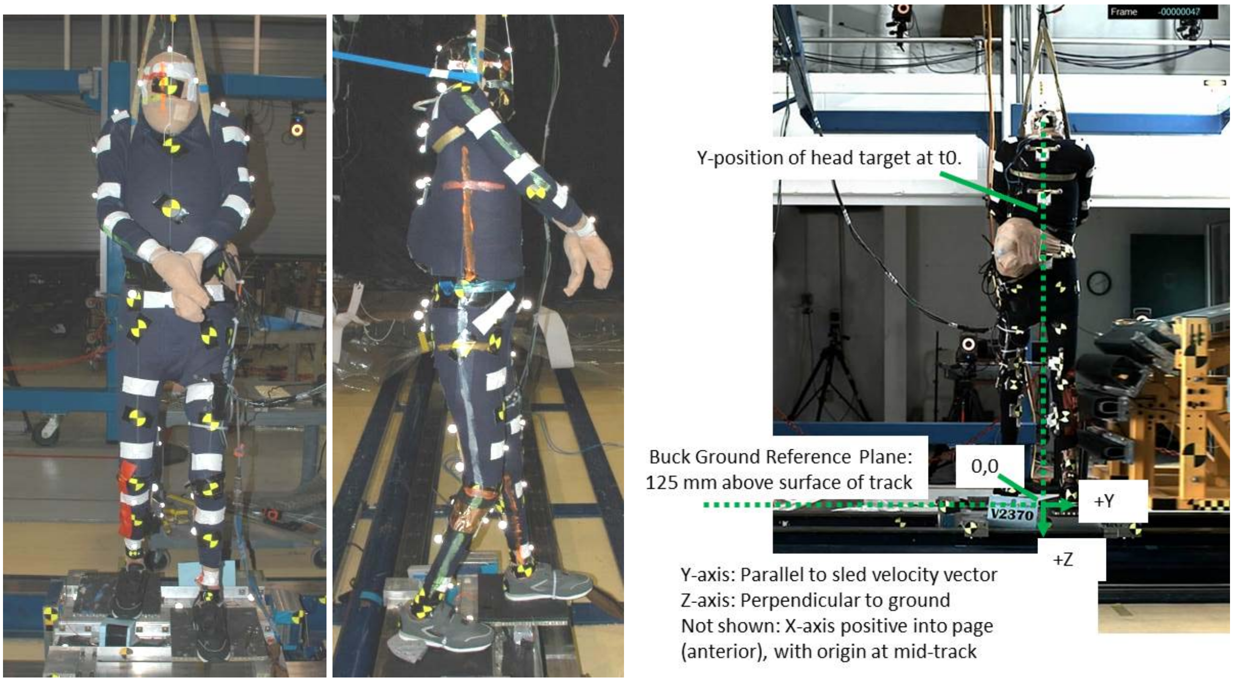

Fig. 2. Left: Initial subject position. Right: Coordinate system used for kinematic trajectory analyses.

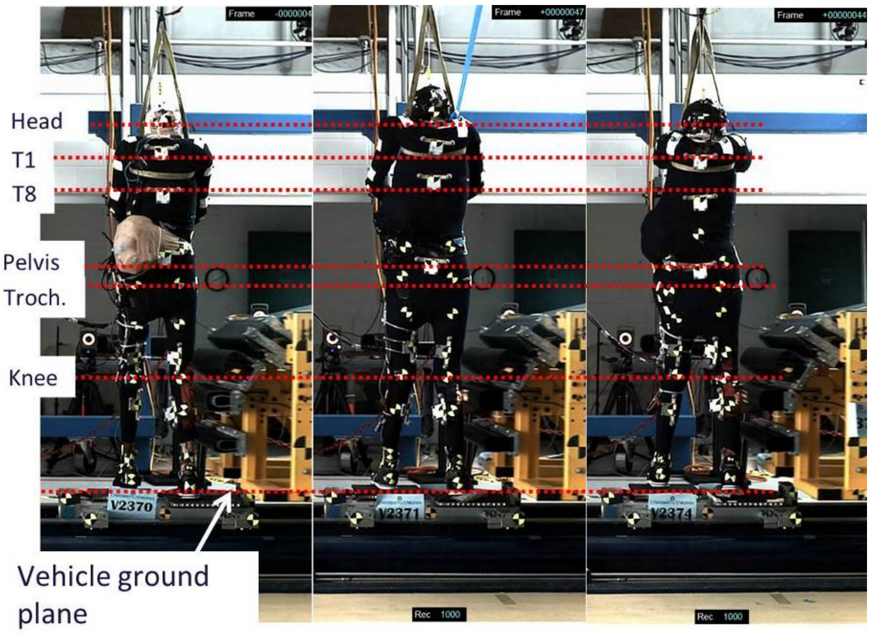

Fig. 3. Knee height alignment. Dashed lines shown as reference for comparison between subjects.

TABLE III
FOOT PLATFORM HEIGHT ADJUSTMENT VALUES

Test #	Height of foot platform relative to buck ground plane (mm)*
V2370	-51
V2371	-39
V2374	-32

* Negative indicates that the foot platform is below the buck ground plane.

Video Tracking

The PMHS kinematics were tracked using a high-speed video imager positioned for a posterior view of the subject. The imager was a Memrecam NAC-GX1 model with a 1280x1024 resolution, a 50 mm Nikkor lens adjusted to a focal length mid-way between 5m and infinity. The imager was placed approximately 6.7 m from the mid-line of the track, and captured 1000 frames per second. Phototargets on the head, T1, T8, and the pelvis were tracked. The coordinate system used for both the video tracking and the Vicon analysis is shown in Figure 2.

The following video tracking and processing steps were taken:

1- Track all target markers to have their positions in pixel units at 1 ms intervals (i.e, every video frame), starting from the time at which the vehicle phototarget entered the video frame (8-11 ms prior to leg contact) and ending 10 ms after head contact.

2- Rotate the coordinate system of the digitized points such that the velocity vector of the vehicle buck and pedestrian sled is aligned with the global Y axis.

3- Extract the initial locations of all targets in 3D space as digitized pre-test by a Romer 3D coordinate measurement device (model RA-7330SI, Hexagon Metrology Inc., North Kingstown, RI). Transform these 3D position measurements to the video tracking XYZ coordinate system (Figure 2).

4- Define pixel-to-mm conversion coefficient (Ci) as a function of X (i.e., as a function of depth into the high-speed video image; Equation 1) using linear interpolation.

$$\frac{C_i - C_1}{C_2 - C_1} = \frac{X_i - X_1}{X_2 - X_1} \qquad (1)$$

where:

- C_i and X_i are the conversion coefficient and X coordinate, respectively, of the i^{th} photo target.
- C_1 is the conversion coefficient determined from the pair of points of known distance apart that define length reference #1. Both of these points must be in the same plane, having an X-coordinate of X_1.
- C_2 is the conversion coefficient determined from the pair of points of known distance apart that define length reference #2 (which is at a different X-plane than length reference #1). Both of these points must be in the same plane, having an X-coordinate of X_2.

Solving the equation above for C_i gives:

$$C_i = \left(\frac{X_i - X_1}{X_2 - X_1}\right)\left(C_2 - C_1\right) + C_1 \qquad (2)$$

5- Determine C_i for each target marker based on its X coordinate which can be found by the initial 3D Romer data. For the purposes of defining the conversion factor, it is assumed that each target remains in the same X-plane as its initial position during the impact.

6- Transform units from pixel to mm for each point using the conversion coefficients C_i defined for each target.

7- Subtract initial video tracking position (Y,Z) of each target to determine change in position (displacement) in time.

8- Determine the initial Y position and Z position of each target in the lab reference frame using the 3D Romer Arm data. [Note: The 3D Romer data is used to define the initial position of each marker in order to account for differences in the location of the global origin in the video frame as a function of the initial X position of each marker.]

9- For each target, add the change in position (displacement) determined from video tracking at each point in time to the initial position determined from the Romer data to determine the trajectory (Y,Z location in time) in the lab reference frame (Figure 2).

10-Subtract the Y displacement of the vehicle (relative to its t_0 position) from the Y position of each target marker at each point in time to determine the relative position/motion of the subject with respect to the vehicle. (Y origin = Y location of the head with respect to the vehicle at the time of leg contact.)

11-Crop the data between the time of leg contact (t_0) and the time of head contact.

Regarding the tracking of the head - being concerned about potential effects of the head on the apparent location of the head photo target, previous studies have used head tracking methods involving digitizing multiple points on the perimeter of the head and combining to estimate the position of the centroid of the head [6]. For this study, in addition to tracking the head phototarget a method to estimate the head centroid location was also used. In each frame 4 additional points on the head were digitized: the top (apex) of the head, the bottom (occiput) of the head, the right side of the head (at mid head-height), and the left side of the head (at mid head-height). The centroid of the head was then estimated as the average of the Y and Z coordinates of each of these 4 points (Figure 4).

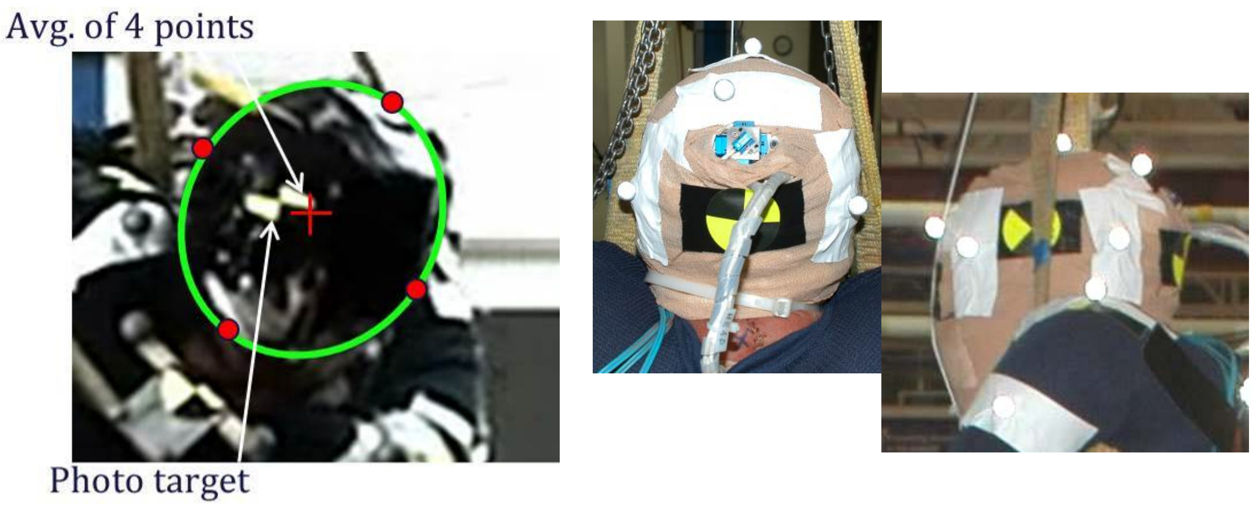

Fig. 4. Left: Head phototarget and average of four perimeter points. Right: Vicon markers arranged around the surface of the head. The motion of these markers was used to calculate the motion of the head center of gravity (c.g.)

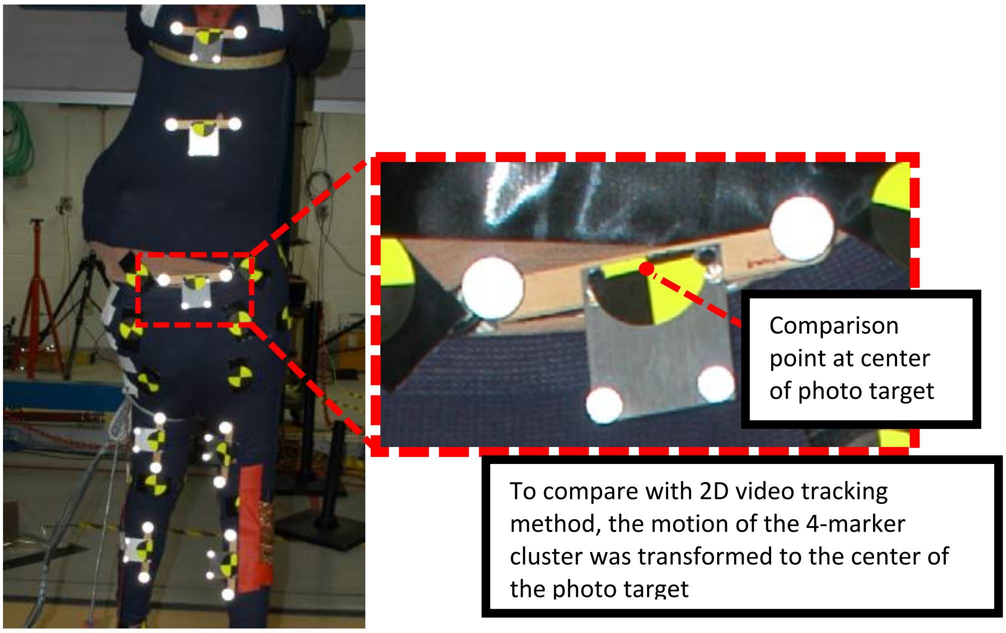

Fig. 5. Phototargets and Vicon arrays

Vicon Tracking

To validate the high speed video tracking methodology, complementary tracking with a Vicon 3D optoelectronic motion capture system was also performed. Twenty-five Vicon motion capture cameras were arranged around a capture volume encompassing the region of interaction between the subject and the buck. These cameras were used to track spherical retroreflective markers attached to the subject and the buck. For T1, T8, the pelvis, and the lower extremities plates containing 4 Vicon markers were rigidly affixed to their respective skeletal mounts via aluminum standoffs. The video-tracking phototargets were also attached to these plates, as shown in Figure 5. For each plate the data from the 4 attached Vicon markers was transformed to calculate the motion of the center of the video-tracking phototarget to facilitate a direct comparison with the 2D video tracking method described above. The buck motion data (as recorded by Vicon) was then subtracted to provide the Vicon-calculated motion of the phototargets relative to the buck reference frame.

For the head, an array of 7 Vicon markers was affixed around the surface of the head (Figure 4). These were transformed to calculate the motion of the nominal head center of gravity (c.g.). The resulting trajectory was then compared to the trajectories calculated from video-tracking of either the head phototarget or the average of 4 points around the perimeter of the head.

Scaling and Corridor Development

To further account for differences in subject height and body segment length, the trajectories were scaled via the length-scaling method outlined by Yanaoka et al. [15]. For each phototarget location a length scale factor was calculated by dividing the knee-to-target height (vertical distance from the struck knee to the phototarget) expected of a 50th percentile male dummy (Table V, SAE J2782) by the knee-to-target height of the PMHSs. For each target the scaled Y-axis position time-history was then calculated by multiplying the unscaled Y-axis position by the length scale factor for that target at each point in time.

The scaled Z-axis position was calculated by:

1- Subtracting the initial ground-to-knee height (vertical distance from the buck ground reference plane to the struck knee at time t_0) from the unscaled Z-axis position of each target at each point in time.
2- Multiplying this re-zeroed Z-axis position by the length scale factor for each target at each point in time.
3- Un-zero and aligning initial positions by adding the initial phototarget height expected of a 50th percentile male dummy as described by SAE J2782.

Trajectory corridors were then developed according the method described in SAEJ2868.

In brief, for each phototarget an average response was first calculated by the following steps:

1- For any data trace containing gaps resulting from a loss of visual contact with the phototarget, the gaps were filled via linear interpolation.
2- To account for differences in time-period between leg strike and head strike between tests, the time-scales of each trace were normalized by dividing the time value of each time step by the time of head contact. [Note that t_0 equals the time of leg contact for each test.] As a result, the normalized time for each test goes from 0 (leg contact) to 1 (head contact).
3- These time-normalized traces were then re-sampled via table-lookup with linear interpolation with 201 equally-spaced normalized timesteps.
4- The mean value between the three tests of scaled Y and scaled Z at each resampled, normalized timestep was then calculated.

For each phototarget a corridor around the mean response was then constructed. Consistent with SAE J2868, the width of the corridor at each point along the mean trajectory was defined based on the path length of the mean trajectory up to that point. The following steps were taken to construct the corridors:

1- Calculate the accumulated path-length as a function of time:

$$S_i = \sum_{j=1}^{i} \sqrt{(\bar{y}_j^* - \bar{y}_{j-1}^*)^2 + (\bar{z}_j^* - \bar{z}_{j-1}^*)^2} \qquad (3)$$

where:

S_i is the total accumulated path length in mm.

$\bar{y}_j^*$ and $\bar{z}_j^*$ are the average scaled *y* and *z* components of the mean trajectory trace being analyzed at the normalized, resampled timepoint *j*

2- Four signals were calculated to determine the corridors. These four signals represent the corners of a square, with a reference point on the average trajectory curve, and whose dimension is equal to $(J+k)S_i$, where J and k are variables representing a percentage of the trajectory's path length S_i. The four signals were calculated as:

$$\begin{aligned} C_{y,i}^{+} &= \bar{y}_i^{*} + k_y S_i \\ C_{y,i}^{-} &= \bar{y}_i^{*} - J_y S_i \\ C_{z,i}^{+} &= \bar{z}_i^{*} + k_z S_i \\ C_{z,i}^{-} &= \bar{z}_i^{*} - J_z S_i \end{aligned} \qquad (4)$$

where $C_{y,i}^{+}, C_{y,i}^{-}, C_{z,i}^{+}, C_{z,i}^{-}$ are the y and z corridor signals for the 4 corners of the percentage path length square.

3- Considering trajectory polarity and concavity, the upper corridor bound for the head, T1 and T8 was defined as the cross-plot of $C_{y,i}^{+}$ and $C_{z,i}^{-}$, and the lower bound was defined as a cross-plot of $C_{y,i}^{-}$ and $C_{z,i}^{+}$. For the pelvis the upper bound was defined as the cross-plot of $C_{y,i}^{-}$ and $C_{z,i}^{-}$, and the lower bound was defined as a cross-plot of $C_{y,i}^{+}$ and $C_{z,i}^{+}$. Consistent with SAE J2868, the corridors were designed to be asymmetric about the mean with a total side length $(J+k)S_i$ equal to 15% of the accumulated path length (SAE J2868). To accomplish this – for the head, T1 and T8 k_y and J_z (the upper bound path-length percentages) were each set to 5%, and J_y and k_z (the lower bound percentages) were each set to 10%. For the pelvis J_y and J_z (upper bound) were set to 10% and k_y and k_z were set to 5%.

4- Once the corridor bounds were calculated, they were resampled with 7 points equally spaced in normalized time for ease of tabulation.

III. RESULTS

Three pedestrian impact tests were performed with three PMHS. The impact velocities of the buck were all within 1.5% of the target impact velocity of 40 km/h, and the suspension release times were consistent within 5 ms of each other (Table IV). Head contact times (after initial leg contact) ranged from 135 ms to 141 ms, and head wrap around distances ranged from 2175 mm to 2200 mm (measured from the buck ground reference plane, *not* the height-adjusted foot plates). High speed video images showing the overall kinematics are included in Appendix C.

TABLE IV
TEST IMPACT VELOCITIES, EVENT TIMES, AND HEAD WRAP-AROUND DISTANCE

Test #	Buck Impact Velocity (km/h)	Suspension Release Time (ms)*	Head Contact Time (ms)*	Head Wrap-Around Distance (mm)**
V2370	40.0	-29	135	2190
V2371	39.4	-30	138	2175
V2374*	40.2	-34	141	2200

* Times relative to the time of leg contact.
** Wrap around distance measured from the height of the buck ground reference plane, *not* from the cadaver foot platform height.

Trajectories of the head, T1, T8, and the pelvis were measured both with video tracking and with Vicon 3D motion capture. These are overplotted in the buck reference frame in Figure 6. The trajectories drawn from video tracking were also scaled via length scale factors derived from knee-to-target heights (Table V). Raw and scaled trajectories are shown in Figure 7. Corridors were then developed (Figure 8), and the points defining the upper and lower bound of each corridor were tabulated (Table VI).

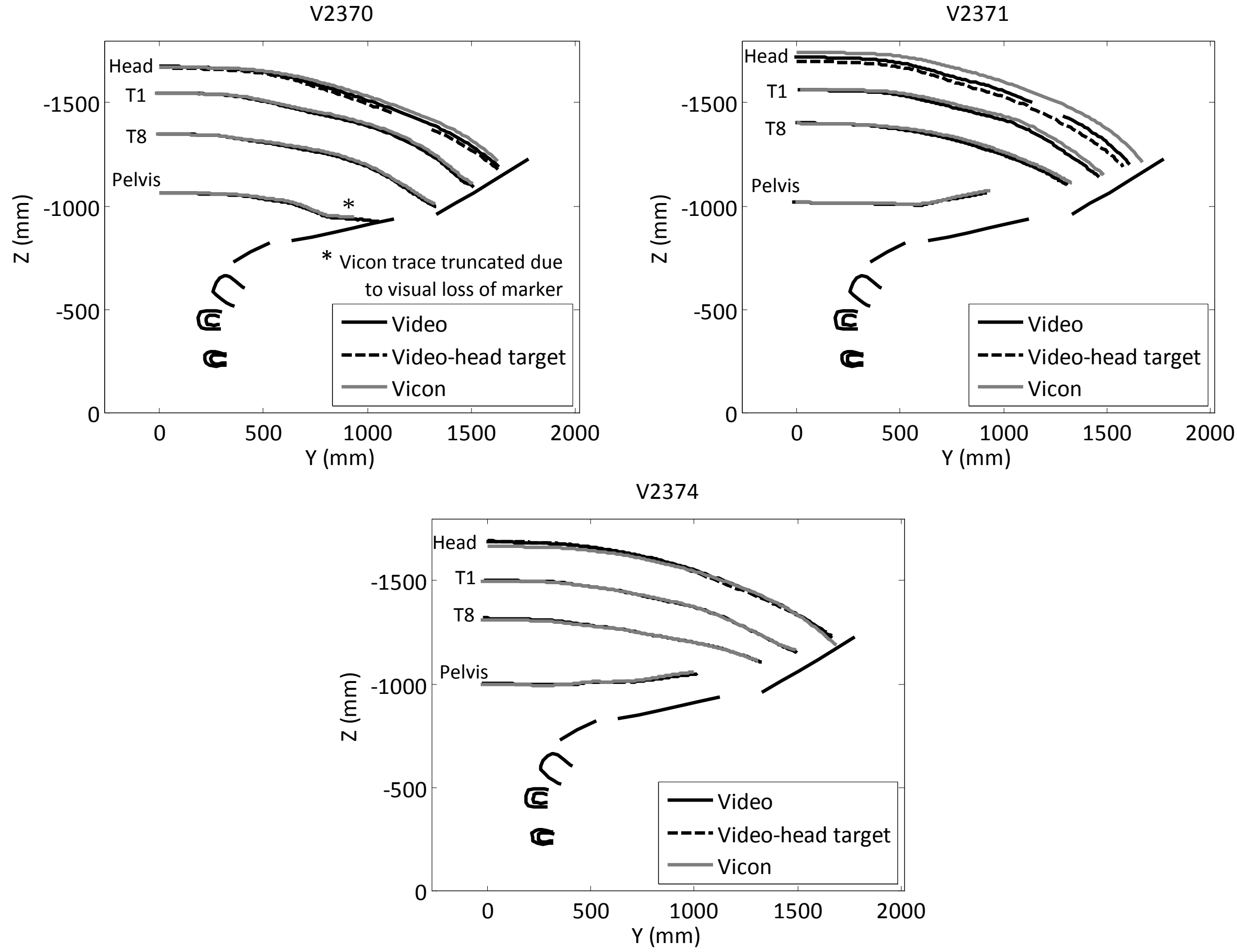

Fig. 6: Video tracking trajectory data vs. Vicon trajectory data (Vicon data transformed to phototarget locations for T1, T8, and the pelvis; and to the head c.g. for the head). For the video tracking data for the head, the solid black line is from the average of four points on the perimeter, and the dashed black line is from the posterior head phototarget.

TABLE V
TARGET-TO-KNEE HEIGHTS AND CORRESPONDING LENGTH SCALE FACTORS

Test #	Height from Struck Knee Target (mm)				Length Scale Factor			
	Head*	T1	T8	Pelvis	Head	T1	T8	Pelvis
Reference	1154	996	847	500	--	--	--	--
V2370	1189	1060	862	578	0.971	0.940	0.983	0.865
V2371	1231	1071	913	529	0.937	0.930	0.928	0.945
V2374	1196	1010	826	511	0.965	0.986	1.026	0.978

* Head is the average of 4 points on the perimeter of the head.

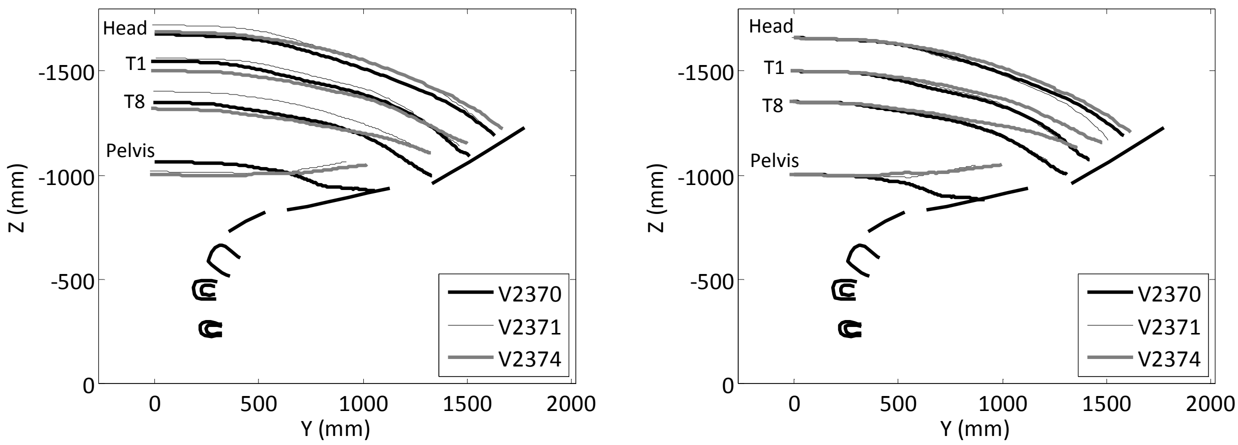

Fig. 7: Video tracking trajectories from each test. Left: Raw. Right: Scaled. The head trajectory for each test comes from the average of four points around the perimeter of the head.

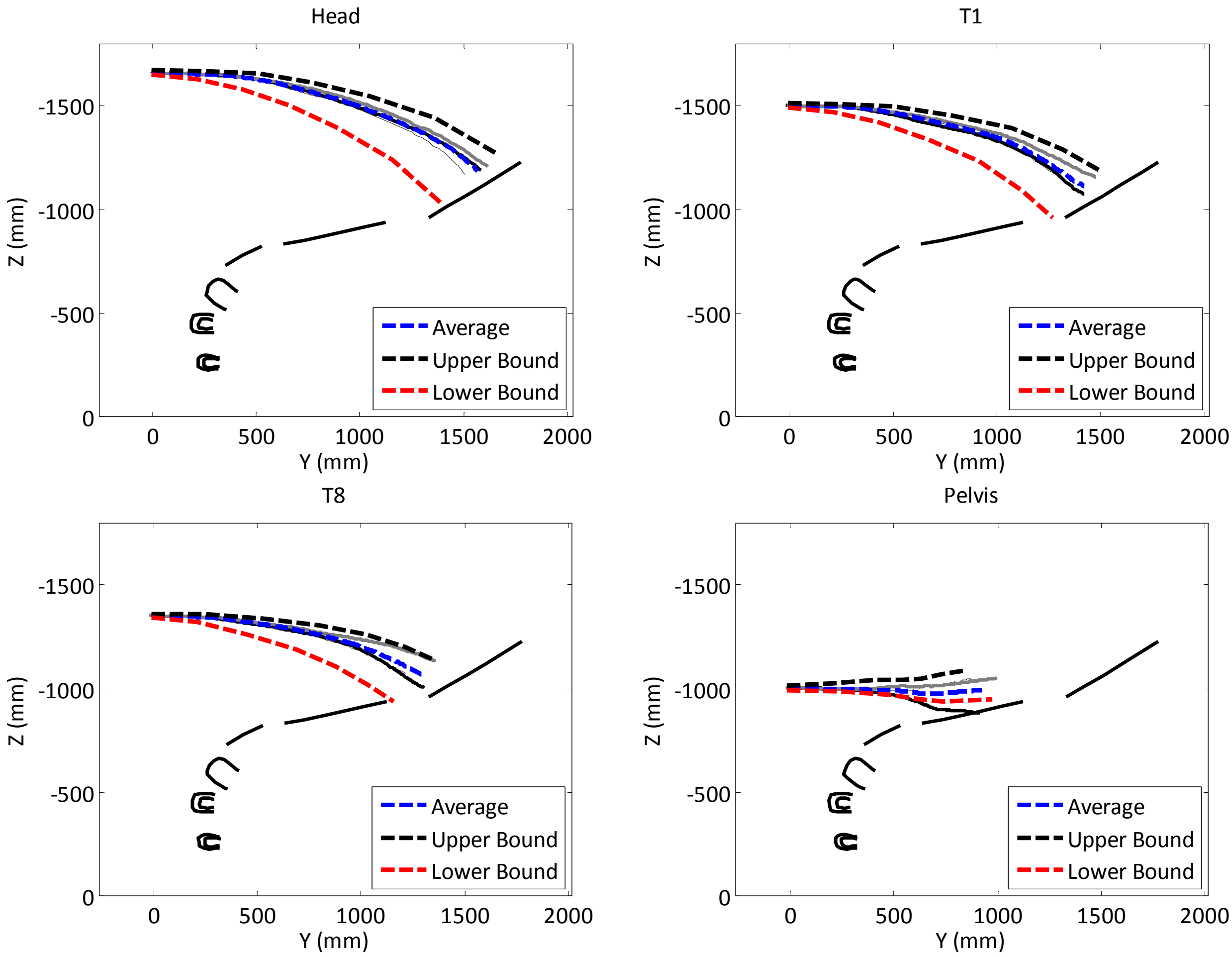

Fig. 8. Trajectory corridors by target location, superimposed on the scaled test trajectories.

TABLE VI
CORRIDOR POINTS*

Head				T1				T8				Pelvis			
Upper		Lower		Upper		Lower		Upper		Lower		Upper		Lower	
Y	Z	Y	Z	Y	Z	Y	Z	Y	Z	Y	Z	Y	Z	Y	Z
-2	-1669	-2	-1649	-8	-1511	-8	-1491	-10	-1362	-10	-1342	-14	-1015	-14	-995
253	-1664	217	-1627	245	-1508	209	-1472	250	-1357	213	-1320	203	-1023	239	-987
510	-1655	437	-1581	504	-1494	431	-1421	529	-1340	451	-1263	409	-1041	479	-971
768	-1612	657	-1501	782	-1450	668	-1336	804	-1307	687	-1190	537	-1042	629	-950
1050	-1547	897	-1394	1069	-1393	912	-1236	1026	-1261	876	-1111	630	-1048	738	-940
1360	-1441	1159	-1240	1316	-1287	1120	-1092	1213	-1199	1034	-1020	726	-1067	849	-944
1653	-1271	1402	-1020	1494	-1189	1268	-963	1361	-1138	1159	-936	832	-1088	973	-947

* All coordinates are in mm.

IV. DISCUSSION

Video Tracking vs. Vicon

The trajectories captured from Vicon tracking were nearly identical to those captured via tracking and analysis of the 2D high speed video for T1, T8, and the pelvis. For those locations the phototarget and the corresponding Vicon marker arrays were mounted rigidly to a common piece of hardware. The Vicon array data was then transformed via rigid body transformation to calculate the 3D motion of the center of the video-tracking phototarget. This allows the most precise direct comparison possible between the Vicon results and video tracking results. The consistency of these results suggests that the 2D video tracking and analysis method accurately captures the subject trajectories projected onto the Y-Z plane.

Some small variation was observed between Vicon trajectories and video tracking trajectories for the head. Considering the consistency observed in the other target sites, it is likely that the variation observed in the head is not due to systematic differences between the video tracking and the Vicon tracking, but is instead due to differences in how the tracking location on the head was defined. Unlike on the other tracking sites, the Vicon markers and phototargets were not co-mounted on the head. Instead, the Vicon markers were mounted to approximate the head c.g. and two different methods were used to track via video (single phototarget on the back of the head and tracking of 4 points on the perimeter of the head). Some of the variation in trajectory is due to differences in initial positions of the tracked points (Figure 6). Some variation also likely results, however, from rotation of the head. As can been seen for V2371, the video tracking technique utilizing four points on the perimeter of the head resulted in a closer match to the Vicon data compared to utilizing the rear head phototarget alone. Using the four points on the perimeter inherently mitigates some of the effect of head rotation, but can also be affected by spherical asymmetry of the head – as the head rotates it projects a different profile onto the Y-Z plane, which may cause some shift in the calculated average of the four points relative to the head c.g.. These differences, however, are small compared to the width of the calculated corridors (typically less than 4%, largest difference 6.5%). Since it gave a more consistent agreement with Vicon, it is recommended that the 4-point perimeter tracking method continue to be used for the head.

It should be noted that this video tracking method relies on having well-defined pre-test measurements of the 3D coordinates of each of the tracked phototargets and length reference markers (including on the sled). This is necessary to define and apply a pixel-to-mm conversion factor as a function of X-position. This is also necessary to define the initial position of each target relative to the global origin. Because of foreshortening, the Y-Z origin appears at different locations in the 2D video image as a function of depth into the image. This must be accounted for when tracking phototargets located at different depths in the image, as the zero-value (i.e. the bias) needed to relate the position of the target to the global origin is different for each target as a function of X-position. It may be possible to define the global origin in pixels as a function of X-position, though in this case the availability of pre-test 3D digitization data made it a simpler matter to define the initial position of each target based on the 3D measurement data. The accuracy of this method was corroborated by comparison to the Vicon data. For similar testing, if pre-test 3D coordinate measurement is not available, some other method must be used to define both the length reference and the origin as a function of X-position, and to relate those references to the X-positions of the targets being tracked.

Kinematic Results Comparison

The foot platform height was adjusted for each test to align the vertical position of the struck knee. Because of this, all three subjects showed a consistent knee height relative to vertical position of the striking bumpers and other buck components. Since the vertical adjustment was designed targeting the knee height expected of a 50th percentile male dummy, it would be expected that a dummy's knee would strike the bumper structures at vertical location similar to these cadavers.

The three tests resulted in similar overall kinematics. Aided by the vertical adjustment for knee height, the wrap-around distance relative to the buck ground reference plane were within 2% for each of the three tests. In addition to the head, the T1 and T8 targets also showed similar trajectories. There was some characteristic difference in the pelvis trajectory for test V2370 caused by a different rotational kinematic about the Z-axis. For tests V2371 and V2374 the pelvis exhibited very little rotation about the Z-axis (Appendix C) with some small rotation in the positive Z direction (meaning the left side of the pelvis moved anteriorly and the right side moved posteriorly). Because of this lack of pelvis rotation, the trajectories for those two tests show the pelvis sliding up along the contour of the hood. In contrast, test V2370 exhibited some rotation of the pelvis in the opposite direction (negative Z-axis, left side moving posteriorly). This tended to drive the phototarget down and into the hood, as shown in the resulting trajectory. It is unknown why this occurred, but may be the result of small deviations in the initial z-axis angle of the pelvis or specific anthropometry or mass distribution of this subject. Despite the difference in pelvis kinematics, the consistency observed in the trajectories of the other phototargets suggests that this did not affect the upper body kinematics in a manner that would affect the resulting corridors. Similarly, although the distal upper extremities of the subject of test V2374 were amputated at the mid-forearm (which also resulted in a shallower initial forearm angle from the support from beneath the axilla), that test resulted in upper body kinematics consistent with the others. Thus, the effects of those differences on the overall kinematic results described here are likely marginal.

The specific test methods used here should be considered when replicating these tests for dummy or model comparison. In these tests the subjects were supported upright via a webbing strap passed under the axilla and around the back. While some pedestrian dummies contain alternative options for lifting and positioning (e.g., hoist points located on the shoulders), the support method used for the PMHS should be replicated with the dummies when performing biofidelity assessment tests. To simplify positioning the arms of the PMHS were bound to each other at the wrist (or at the point of amputation for test V2374). This also reduces the potential range of kinematics that can occur - for example, limiting the propensity for the struck-side arm to become trapped between vehicle and torso. Thus, this constraint should also be replicated in any dummy or model biofidelity assessment tests. Finally, the primary goal of this study was to provide kinematic trajectory information specifically for the assessment of pedestrian dummies to augment the recommendations currently present in SAE J2868. As dummy trajectories are typically tracked via phototargets placed on the exterior surface of the dummy (usually observed via 2D high-speed video), the trajectories described for the PMHS are based on phototargets placed on the external surface of the subjects (for all locations except the head). As a result, however, the apparent motions are affected by out-of-plane rotations of the body segments (for example, the rotation of the pelvis). Alternatively, the Vicon 3D motion tracking data captured in this study may facilitate tracking of the motion and rotation of anatomically-defined landmarks within the various body segments. While beyond the scope of this specific paper, such 3D kinematic data may facilitate detailed evaluation of pedestrian human body computational models in the future.

Scaling and Corridors

Since the subjects were all very similar in anthropometry to each other, they tended to exhibit very similar trajectories without needing scaling. Despite this consistency, the subjects were all taller than what would be expected of a 50th percentile male dummy. Thus scaling is still required to transform these trajectories into what would be expected of a dummy.

By design, the scaling resulted in a consistent vertical alignment of the initial target locations. The scaling also resulted, however, in a small increase in the dispersion of the endpoints of the trajectories. Despite this, the scaled trajectories still tended to fall within the resulting corridors, suggesting that the scaled trajectories represent a reasonable range of variation. The only scaled trajectory that passed out of its corridor was that of the pelvis of test V2370, which had a somewhat different path-shape due to the aforementioned rotation of the pelvis.

The factors influencing the corridor method development in J2868 remain present in the current study. Thus this study used the same corridor construction techniques. As with the subjects in J2868, the current PMHS are all taller than the 50th percentile male. Even though the subjects were vertically aligned at the knee, differences in stature or femur length may still affect the interaction between the pelvis and hood leading edge (and thus affect upper body kinematics) in a manner similar to that described in J2868. As with all PMHS, the current subjects also exhibit the same lack of active musculature effects as the subjects in the original study. These two factors formed the basis of the reasoning leading to the asymmetric corridor definition, and are as applicable now as they were then.

Overall, the scaled trajectory corridors developed here are similar to the trajectory corridors developed by Kerrigan et al. [10] for similar 40 km/h pedestrian testing utilizing a mid-sized sedan (also the basis for the corridors currently used in SAE J2868). For example, in the current study the Y-Z coordinates for the endpoint of the head trajectory are (1653,-1271) mm for the upper bound and (1402,-1020) mm for the lower bound. After correcting for differences in polarity definition, the corresponding points from the current SAE J2868 are (1650,-1330) mm for the head upper bound and (1370,-1030) mm for the lower bound. In other words, the differences are less than 3% at the endpoint of the head trajectory. Similar consistency was observed in the other trajectory corridors, with endpoint coordinate differences ranging from 0.4% to 6%. This is curious considering that those corridors were developed using a different vehicle platform, consisting of the front end of an actual production vehicle (2004 four-door Honda Civic). This suggests that the generic vehicle buck used in the current study results in similar subject kinematics to that particular vehicle under these test conditions.

Combined with the generic vehicle buck platform, the scaled trajectory corridors developed here provide a means to assess overall kinematic biofidelity of a 50th percentile male dummy without the need to obtain and test with a specific production vehicle. Furthermore, the comparative analysis demonstrates that when performed properly, 2D video tracking can be used to accurately record Y-Z trajectories even when target points are located at different planes within the X-dimension (depth) of the image. Thus, laboratories that do not possess 3D motion capture equipment may be able to replicate these tests and compare dummy trajectories to these corridors using 2D motion tracking alone. In addition to providing data and methods for dummy kinematic evaluation, these data may be used for the evaluation and refinement of human body computer models developed for assessing injury risk and vehicle interaction in pedestrian impacts. For such evaluations, kinematic comparison may be extended from simple 2D analysis to comparison of 3D motion and rotations using the motion capture data collected here.

V. CONCLUSIONS

Three 40 km/h pedestrian impact tests were performed with adult male PMHS. Trajectories of the head, T1, T8 and the pelvis were tracked via 2D video analysis and 3D optoelectronic motion capture. The trajectories resulting from the 2D video tracking were consistent with those derived from the 3D motion capture, suggesting that these 2D video tracking techniques may be used in lieu of 3D motion capture when such capability is not available. The trajectory results were then scaled and corridors were developed. Combined with the generic vehicle buck and validated trajectory capture and analysis method, these results provide a means to evaluate the whole body kinematic biofidelity of 50th percentile male pedestrian dummies and computational models in perpetuity.

VI. REFERENCES

[1] World Health Organization. *Global Status Report on Road Safety*, 2013.

[2] European New Car Assessment Programme. *Pedestrian Testing Protocol*, Version 5.3.1, November 2011.

[3] Kerrigan J R, Crandall J R, Deng B. A comparative analysis of the pedestrian injury risk predicted by mechanical impactors and post mortem human surrogates. *Stapp Car Crash Journal*, 52:527-567, 2008.

[4] Crandall J, Wiley K, Longhitano D, Akiyama A. Development of performance specifications for a pedestrian impact dummy. *Proceedings of the 19th International Technical Conference on the Enhanced Safety of Vehicles (ESV)*, paper no. 05-0389, Washington, D.C., 2005.

[5] Society of Automotive Engineers Human Biomechanics And Simulation Standards Steering Committee. *Performance Specification for a Midsize Pedestrian Research Dummy, Surface Vehicle Information Report J2782*, 2010.

[6] Society of Automotive Engineers Human Biomechanics And Simulations Standards Steering Committee. *Pedestrian Dummy Full Scale Test Results and Resource Materials, Surface Vehicle Information Report J2868*, 2010.

[7] Pipkorn B, Fredriksson R, Oda S, Takahashi Y, Suzuki S, Ericsson M. Development and validation of a generic universal vehicle front buck and a demonstration of its use to evaluate a hood leading edge bag for pedestrian protection. *Proceedings of the International Research Council on the Biomechanics of Impact (IRCOBI)*, p. 168-181, Dublin, Ireland, 2012.

[8] Pipkorn B., Forsberg C., Takahashi Y., Ikeda M., Fredriksson R., Svensson C., Thesleff A. Development and component validation of a generic vehicle front buck for pedestrian impact evaluation. *Proceedings of the International Research Council on the Biomechanics of Impact (IRCOBI)*, p. 718-729, Berlin, Germany, 2014.

[9] Takahashi Y et al. Full-scale validation of a generic buck for pedestrian impact simulation. *Proceedings of the International Research Council on the Biomechanics of Impact (IRCOBI)*, p. 730-745, Berlin, Germany, 2014.

[10] Kerrigan J R, Murphy D B, Drinkwater D C, Kam C Y, Bose D, Crandall J R. Kinematic corridors for PMHS tested in full-scale pedestrian impact tests. *Proceedings of the 19th International Technical Conference on the Enhanced Safety of Vehicles (ESV)*, paper no. 05-0394, Washington, D.C., 2005.

[11] Kam C Y et al. Design of a full-scale impact system for analysis of vehicle pedestrian collisions. *Society of Automotive Engineers*, paper no. 2005-01-1875, Detroit, Michigan, 2005.

[12] Shaw G, Parent D, Purtsezov S, Lessley D, Crandall J, Kent R. Impact response of restrained PMHS in frontal sled tests: skeletal deformation patterns under seat belt loading. *Stapp Car Crash Journal*, 53:1-48, 2009.

[13] Lessley D, Shaw G, Riley P, Forman J, Crandall J. Assessment and validation of a methodology for measuring anatomical kinematics of restrained occupants during motor vehicle collisions. *Journal of Biosensors and Bioelectronics*, S1, 2011.

[14] Forman J L et al. Occupant kinematics and shoulder belt retention in far-side lateral and oblique collisions: a parametric study. *Stapp Car Crash Journal*, 57:343-385, 2013.

[15] Yanaoka T, Torikai K, Ikeda M. Takahashi Y. Investigation of the influence of the aligned height on the scaled whole body trajectories in car-to-pedestrian collisions. *International Journal of Automotive Engineering* (in press).

VII. APPENDIX

Appendix A: Subject anthropometry (all dimensions in mm)

Supine Anthropometry			
Cadaver ID No.	724	727	756
Stature	1795	1870	1780
Vertex-to-Symphision Length	855	930	860
Top-of-Head to Trochanterion	825	910	880
Shoulder (Acromial) Height	1555	1620	1550
Waist Height (at Umbilicus)	1090	1123	1070
Waist Depth (at Umbilicus)	180	190	190
Waist Breadth – Umbilicus	313	350	341
Waist Breadth - Bitrochanteric	332	390	358
Waist Breadth - Bicristal	294	340	356
Shoulder Breadth (Biacromial)	393	344	381
Chest Breadth – 4th Rib	321	331	306
Chest Breadth – 8th Rib	319	335	316
Chest Depth – 4th Rib	235	230	213
Chest Depth – 8th Rib	240	220	235
Buttock Depth	163	170	175
Shoulder-to-Elbow	390	370	355
Forearm-to-Hand	487	500	153*
Elbow-to-Stylion	290	300	NA
Tibiale Height	490	500	500
Trochanter Height	952	995	935
Iliocristale Height	1100	1140	1030
Ankle Height (Outside)	92	90	88
Foot Breadth	90	87	86
Foot Length	238	280	221
Head Length	185	205	198
Head Breadth	161	157	158
Head Height	214	250	215
Head Circumference	583	580	592
Neck Circumference	452	352	445
Chest Circumference – 4th Rib	1145	938	970
Chest Circumference – 8th Rib	955	928	975
Waist Circumference – At Umbilicus	890	904	925
Waist Circumference – 8cm above Umbilicus	910	913	985
Waist Circumference – 8 cm below Umbilicus	861	900	916
Buttock Circumference	915	1010	1030
Thigh Circumference	493	565	566
Lower Thigh Circumference	323	510	390
Knee Circumference	349	380	386
Calf Circumference	282	305	317
Max Lower Leg Breadth	85	107	93
Ankle Circumference	190	245	238
Scye (Armpit) Circumference	402	345	333
Bicep Circumference	247	265	275
Elbow Circumference	239	254	258
Forearm Circumference	226	233	210*
Wrist Circumference	165	175	NA
Shod R. Knee Height (bottom of foot to knee, outside)	585	570	565

Standing Anthropometry			
Cadaver ID No.	724	727	756
Chest Breadth	321	330	293
Iliac Breadth	293	361	381
High Thigh Breadth	143	152	157
Mid Thigh Breadth	118	129	118
Maximum Lower Leg Breadth	92	104	109
Middle Lower Leg Breadth	66	77	79
Head Length	221	230	219
Chest Depth	246	208	242
Abdominal Extension Depth (Iliocristale)	237	267	255
High Thigh Depth	132	173	149
Mid Thigh Depth	128	146	138
Maximum Lower Leg Depth	110	103	102
Mid Lower Leg Depth	93	75	88
Mid Arm Breadth	75	85	90
Forearm Breadth	66	73	89
Mid Arm Depth	86	80	95
Forearm Depth	65	72	89
Head Circumference	642	650	680
Chest Circumference	930	890	898
Abdominal Circumference	919	NM**	NM**
Buttock Circumference	955	1030	955
High Thigh Circumference	499	530	510
Mid Thigh Circumference	395	475	415
Calf Circumference	334	362	327
Mid Leg Circumference	220	265	260
Mid Arm Circumference	270	260	310
Mid Forearm Circumference	235	245	300

** NM = Not Measured

Appendix B: Initial position measurements

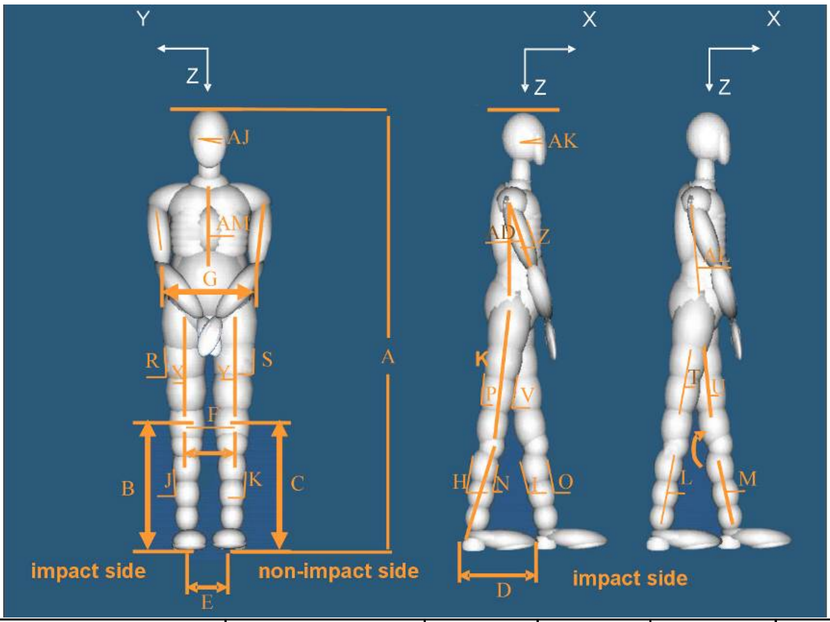

	Segment	Aspect	Units	Axis†	V2370	V2371	V2374
A	Height*		mm	Z	1830	1885	1810
B	Knee Height*	Impact Side	mm	Z	545	531	535
C		Non-Impact Side	mm	Z	545	553	555
D	Heel To Heel Distance		mm	X	270	382	381
E			mm	Y	255	239	291
F	Knee To Knee width		mm	Y	202	219	228
G	Elbow To Elbow Width		mm	Y	382	562	412
H	Tibia Posterior	Impact Side	deg	Y	73.6	69.3	69
I		Non-Impact Side	deg	Y	90.7	99.4	100.6
J	Tibia Lateral	Impact Side	deg	X	84.1	85	81
K		Non-Impact Side	deg	X	93.6	95.2	92.3
L	Tibia Lateral (mid-knee	Impact Side	deg	Y	75.6	65	60.2
M	to lateral malleolus)	Non-Impact Side	deg	Y	84.3	96	96.9
N	Tibia Anterior	Impact Side	deg	Y	89.7	62.3	61
O		Non-Impact Side	deg	Y	82.1	97.2	92
P	Femur Posterior	Impact Side	deg	Y	92.6	105.5	91
Q		Non-Impact Side	deg	Y	101.7	104.6	97
R	Femur Lateral	Impact Side	deg	X	93.7	93.8	86
S		Non-Impact Side	deg	X	85.3	86.6	90.9
T	Femur Lateral (greater	Impact Side	deg	Y	95.4	94.1	96.7
U	trochanter to knee)	Non-Impact Side	deg	Y	114.4	100.1	97.3
V	Femur Anterior	Impact Side	deg	Y	90.9	85.6	89
W		Non-Impact Side	deg	Y	99.3	98.8	97.9
X	Femur Anterior	Impact Side	deg	X	89.6	94.4	88.8
Y	(centerline)	Non-Impact Side	deg	X	94.2	88.5	93.1
Z	Humerus Anterior	Impact Side	deg	Y	62.5	49.4	16.7
AA		Non-Impact Side	deg	Y	58.9	54.1	10.3
AD	Humerus lateral (acrom.	Impact Side	deg	Y	63.7	52.6	12
AE	to lat. epicondyle)	Non-Impact Side	deg	Y	57.8	56.7	10.9
AJ	Head Angle**	(bi-orbital)	deg	X	0.5	0.5	3.2
AK		(Frankfort plane)	deg	Y	-2.5	-4.2	5.1
AL	Torso Angle	(acromion-troch.)	deg	Y	98.8	85.6	94.8
AM		(centerline)	deg	X	-3.4	-5.1	5.6

* All height measurements from the top of the foot platform for each particular subject.
** Positive is nose up, left ear down.
† Distance: measurement taken paralell to listed axis. Angles: measurement taken about (i.e., rotated around) the listed axis.
NM = Not measured.

Appendix C: Still captures from the high speed video

Test V2370 Test V2371 Test V2374

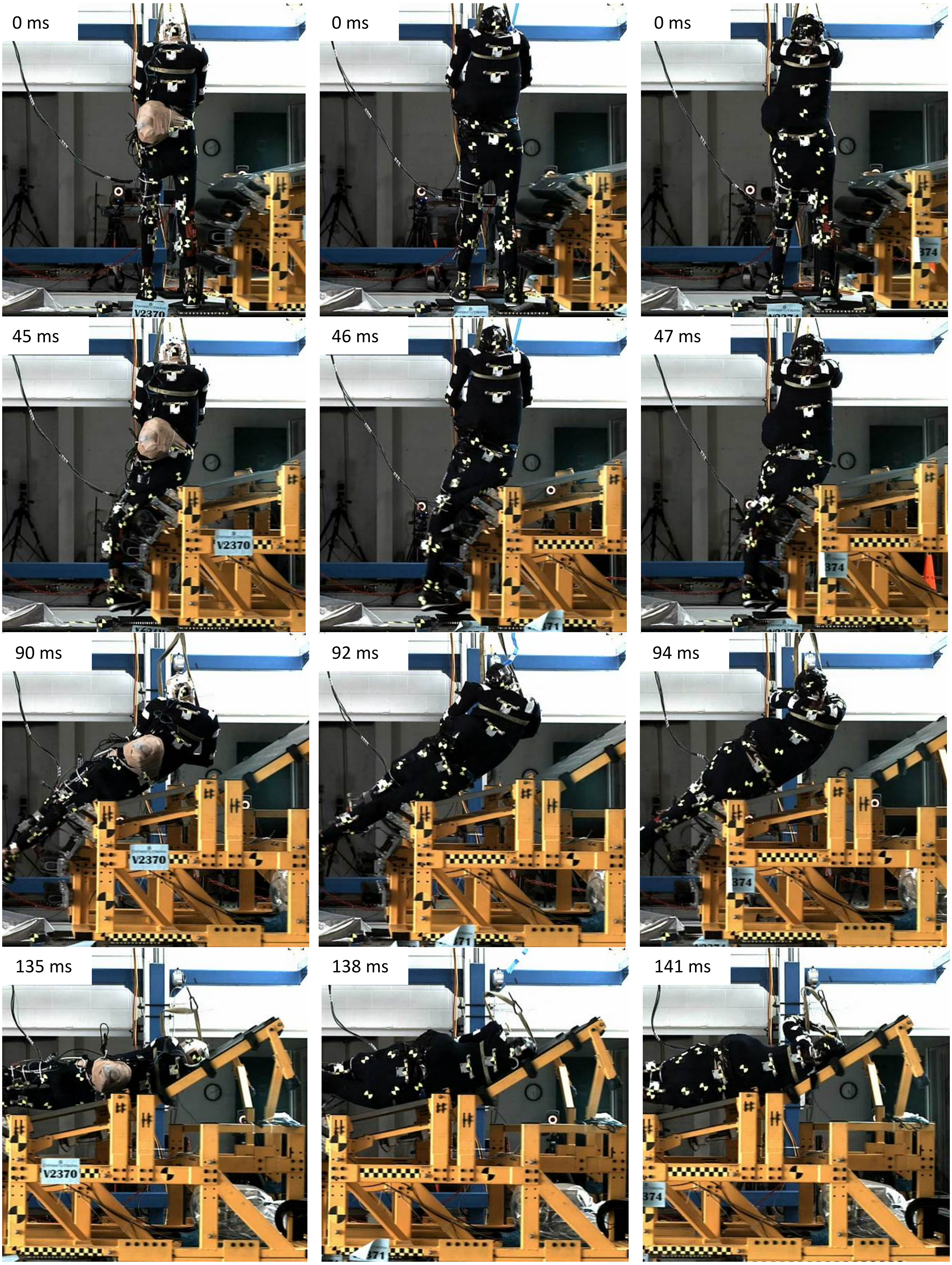

First frame is the frame of leg contact. Final frame is the frame of head contact. Intermediate frames are chosen at even intervals between the two.